JOURNAL OF GEOPHYSICAL RESEARCH, VOL. 114, A07308, doi:10.1029/2009JA014072, 2009



# Latitudinal dependence of the ionospheric response to solar eclipses

Huijun Le,[1,2] Libo Liu,[1] Xinan Yue,[1] Weixing Wan,[1] and Baiqi Ning[1]

Received 14 January 2009; revised 17 May 2009; accepted 26 May 2009; published 16 July 2009.

[1] In this study, we statistically analyze the latitudinal dependence of F2-layer peak electron densities (NmF2) and total electron content (TEC) responses to solar eclipses by using the ionosonde observations during 15 eclipse events from 1973 to 2006 and the GPS TEC observations during six solar eclipse events from 1999 to 2006. We carried out a model study on the latitudinal dependence of eclipse effects on the ionosphere by running a theoretical ionospheric model with the total eclipse occurring at 13 latitudes from 0°N to 60°N at intervals of 5°. Both the observations and simulations show that the NmF2 and TEC responses have the same latitudinal dependence: the eclipse effects on NmF2 and TEC are smaller at low latitudes than at middle latitudes; at the middle latitudes (>40°), the eclipse effect decreases with increasing latitude. The simulations show that the smaller NmF2 responses at low latitudes are mainly because of much higher heights of hmF2 at low latitudes and electron density response decreasing rapidly with increasing height. For the eclipse effects at the middle latitudes (>40°), the simulations show that the smaller NmF2 or TEC response at higher latitude is mainly ascribed to the larger downward diffusion flux induced by the larger dip angle at this region, which can partly make up for the plasma loss and alleviate the depression of electron density in the F region. The simulated results show that there is an overall decrease in electron temperature throughout the entire height range at the middle latitude, but for the low latitudes the eclipse effect on electron temperature is much smaller at high heights, which is mainly because of the much smaller reduction of photoelectron production rate at its conjugate low heights where only a partial eclipse with small eclipse magnitude occurs.

**Citation:** Le, H., L. Liu, X. Yue, W. Wan, and B. Ning (2009), Latitudinal dependence of the ionospheric response to solar eclipses, *J. Geophys. Res.*, *114*, A07308, doi:10.1029/2009JA014072.

## 1. Introduction

[2] The ionospheric responses to a solar eclipse have been studied extensively with various methods, such as the Faraday rotation measurement, ionosonde network, incoherent scatter radar (ISR), Global Positioning System (GPS), and satellite measurements [e.g., *Evans*, 1965a, 1965b; *Klobuchar and Whitney*, 1965; *Rishbeth*, 1968; *Hunter et al.*, 1974; *Oliver and Bowhill*, 1974; *Cohen*, 1984; *Salah et al.*, 1986; *Tsai and Liu*, 1999; *Afraimovich et al.*, 1998, 2002; *Davis et al.*, 2000, 2001; *Farges et al.*, 2001, 2003; *Tomás et al.*, 2007] as well as theoretical modelling [*Stubbe*, 1970; *Müller-Wodarg et al.*, 1998; *Boitman et al.*, 1999; *Le et al.*, 2008a]. These studies have shown that there is an almost consistent behavior at low altitudes where there are larger depletions in electron concentration and electron temperature during solar eclipses and these variations at low altitudes are almost synchronous with the solar radiation variation. The largest relative change in electron concentration (Ne) occurred at the F1 layer heights [*Le et al.*, 2008a]. The F2 layer at middle latitudes is thought to be largely controlled by plasma diffusion. The F2 layer behaviors during solar eclipses may be quite different. They may be accompanied with various amplitudes of decreases or even a small increase in the electron concentration [*Evans*, 1965b; *Salah et al.*, 1986].

[3] As is known, ionospheric plasma behaviors have distinct latitudinal dependence. The magnetic equatorial and low-latitude ionospheric plasma behaviors are dominated by the fountain effect. In the daytime, the vertical E × B drift transports the plasma over the geomagnetic equator from low altitudes to higher altitudes, which causes the much higher F2 layer peak height at the magnetic equator than at the two sides of the region. The lifted plasma diffuses along the magnetic field line to both sides of the equator to form two peak plasma densities at magnetic latitude ±∼15 degrees, which is the famous equator ionization anomaly (EIA). These electrodynamical processes also have important effects on the low-latitude ionospheric responses to solar eclipse [*Cheng et al.*, 1992; *Tsai and Liu*, 1999; *Sridharan et al.*, 2002; *Tomás et al.*, 2007; *Adeniyi et al.*, 2007]. On the basis of GPS TEC data from five GPS

[1]Beijing National Observatory of Space Environment, Institute of Geology and Geophysics, Chinese Academy of Sciences, Beijing, China.
[2]Graduate School of the Chinese Academy of Sciences, Beijing, China.


0148-0227/09/2009JA014072$09.00

stations at low latitude, *Tsai and Liu* [1999] suggested that the fountain effect is essential in explaining the features of the latitudinal location, occurrence time, and amplitude of the major decrease in TEC for the two solar eclipse events: 24 October 1995 eclipse and 9 March 1997 eclipse. *Sridharan et al.* [2002] carried out a case study during 11 August 1999 dusk time total solar eclipse over India and they suggested that the large increase in F-region virtual height immediately after the eclipse was caused by a larger post sunset vertical drift which was induced by the sudden removal of the E-region loading of the F-region dynamo during the solar eclipse. *Tomás et al.* [2007] analyzed the measurements of ionospheric and thermospheric parameters obtained by the Challenging Minisatellite Payload (CHAMP) satellite during the solar eclipse on 8 April 2005 and found that the plasma fountain at the equator was strongly enhanced, resembling postsunset conditions. On the basis of the analysis of the temporal variations of foF2 and electron density above 200 km, *Cheng et al.* [1992] suggested that the variations of the F2 layer around the equatorial anomaly region are controlled not only by the local solar radiation but also by the solar radiation at the equator and the fountain effect plays an important role even during the solar eclipse.

[4] In addition, at middle-high latitudes, the larger magnetic dip angle would result in the larger vertical plasma diffusion flux from the top ionosphere, which would also affect the solar eclipse effect on the F2 layer. *Evans* [1965b] found an increase in foF2 followed by a decrease at three ionosonde stations during the 20 July 1963 total solar eclipse and this increase feature was attributed to the large downward plasma diffusion flux from the top ionosphere caused by the large magnetic dip angles at these stations. *Salah et al.* [1986] suggested the Ne increase above 400 km at near maximum obscuration time was a result of the contraction of the plasma caused by the marked decrease in Te. *Le et al.* [2008b] studied the dip angle effect on the basis of the data derived from 23 ionosonde stations during seven eclipse events and then modeled the dip angle effect by a theoretical ionosphere model. The results show that the larger dip angle would cause the larger downward diffusion flux which makes up the ion losses and subsequently results in the smaller changes in electron concentration in the F region. In addition, *Le et al.* [2009] reported that there were distinct ionospheric disturbances including decrease in electron temperature, increase in foF2 and uplift in hmF2, in the magnetic conjugate points of the eclipse regions during the 3 October 2005 total solar eclipse.

[5] In this study, we statistically analyzed the latitudinal dependence of solar eclipse effect on the ionosphere on the basis of ionosonde observations during fifteen eclipse events from 1973 to 2006 and the GPS TEC observations during six eclipse events from 1999 to 2006. To further study the latitudinal dependence we modeled the solar eclipse effect on the ionosphere by using a theoretical ionosphere model [*Yue et al.*, 2008a] with the total eclipse occurring at thirteen latitude regions from 0°N to 60°N at intervals of 5°, respectively. In order to identify the E × B vertical drift effect on the low-latitude ionosphere's response to the solar eclipse we modeled the eclipse effect in the low latitude without considering the E × B drift.

## 2. Ionospheric Observations

[6] To statistically analyze the latitudinal dependence of F2-layer peak electron densities (NmF2) responses to solar eclipses, we select ionosonde observations during fifteen eclipse events from 1973 to 2006. First, the F2 layer critical frequency (foF2) data from the ionosonde measurements are transformed to the NmF2 data according to the formula $foF2 = 9NmF2^{1/2}$. To ensure that decrease in electron concentration caused by an eclipse was large in comparison with background ionospheric variability, we only considered those observatories with the obscuration at 200 km larger than 50%. The typical way to identify the solar eclipse effect is to examine the deviation of the NmF2 on the eclipse day from that on the reference day, which is written as ΔNmF2. Meanwhile, for better comparison of solar eclipse effect in different latitude regions, the percentage change in NmF2, PNmF2, which is the ΔNmF2 divided by its reference NmF2 in percentage, is also calculated. In this study, the monthly median is taken as the reference value for each observation. In this study, the value of PNmF2 for each observation is negative because of the solar eclipse effect. The largest absolute value of PNmF2, |PNmF2| corresponds to the largest eclipse effect on the F2 layer. For each observation, the largest value of |PNmF2| during the solar eclipse is chosen to describe the F2 layer response to the eclipse. All observations during the corresponding eclipse events lie in the partial eclipse region and the largest obscuration at these stations varies from 51% to 92%. Under the same geophysical conditions, the strength of eclipse effect on NmF2 induced by a partial eclipse can be assumed to be proportional to the masked percentage of solar radiation. For the sake of convenient comparison, under this assumption for each observation event we converted the change in NmF2 induced by a partial eclipse, $PNmF2_P$, into the corresponding change in NmF2 induced by a total eclipse, $PNmF2_T$. The equation for the conversion can be written as follows.

$$PNmF2_T = \frac{PNmF2_P}{\Delta S_P} \tag{1}$$

[7] Here $\Delta S_P$ is the maximum obscuration during an eclipse. The geomagnetic latitude is more useful for the examining the dynamics and mechanism during solar eclipses. Thus to study the latitudinal dependence of solar eclipse effects on the ionosphere, we adopt the geomagnetic latitude in this study.

[8] To further analyze the latitudinal dependence of solar eclipse effects on the ionosphere, we select GPS TEC observations during six solar eclipse events from 1999 to 2006. To normalize the response amplitude we converted the slant TEC to an equivalent vertical value. To decrease the conversion error and avoid other undesired noises, the cut off elevation angle of the GPS receiver in this study was set to be 40 degrees. The TEC data analysis process is the same as that for the NmF2. First, we calculated the deviation of the TEC on the eclipse day from that on the reference day, which is written as ΔTEC. Then the

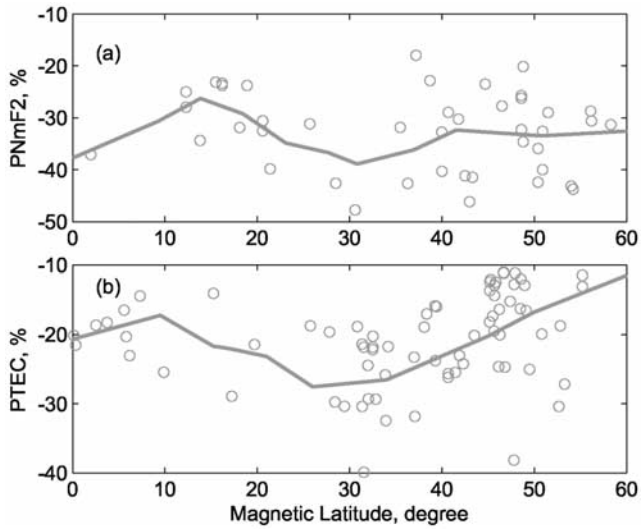


**Figure 1.** Latitudinal dependencies of observed eclipse effects on (a) NmF2 and (b) TEC. The NmF2 data are derived from the ionosonde observations during 15 eclipse events from 1973 to 2006. The TEC data are derived from the GPS TEC observations during six solar eclipse events from 1999 to 2006. Two thick solid lines are the curve fitting of the data of NmF2 and TEC.

percentage change in TEC, PTEC, which is the $\Delta$TEC divided by its reference TEC in percentage, was calculated. All of the observations during the corresponding eclipse events have the largest obscuration at the height of 300 km larger than 50%. The partial eclipse effects were normalized to the total eclipse effects and the maximum of |PTEC| is used to describe the eclipse effect on the TEC for each observation.

[9] On the basis of these converted data, we plotted the latitudinal dependencies of PNmF2 and PTEC in Figures 1a and 1b, respectively. As shown in Figure 1a, there is a distinct latitudinal variation in solar eclipse effect on NmF2: the largest eclipse effect in NmF2 occurs at middle latitudes of $\sim 30^\circ$ and the smallest eclipse effect on NmF2 occurs at low latitudes of $\sim 15^\circ$ where is the EIA region. Figure 1b shows that the TEC data also have these two features. In addition, we also can see that for the middle latitude regions with latitude larger than 35 degrees, the TEC response decreases distinctly with increasing latitude. However, the NmF2 data do not have so distinct tendency.

## 3. Ionospheric Model

[10] On the basis of previous works [*Zhang et al.*, 1993; *Tu et al.*, 1997; *Liu et al.*, 1999; *Lei et al.*, 2004a, 2004b], we develop a middle and low-latitude theoretical ionospheric model, named as: Theoretical Ionospheric Model of the Earth in Institute of Geology and Geophysics, Chinese Academy of Sciences (TIME-IGGCAS). This model adopts an eccentric dipole approximation to the Earth's magnetic field. It solves the coupled equations of the mass continuity, momentum, and energy of three main ions $O^+$, $H^+$ and $He^+$ in closed geomagnetic tubes with their footpoints anchored at about 100 km altitude to yield values of concentrations, temperature, and field-aligned diffusion velocities of these three main ions as well as electrons. The model also calculates the values of concentrations of three minor ions $N_2^+$, $O_2^+$ and $NO^+$ under the assumption of photochemical equilibrium.

[11] The production rates of ions include the photoionization rates and chemical reaction production rates. The solar EUV radiation spectrum reported by *Richards et al.* [1994] is used to calculate the photoionization rates of neutral gas $O_2$, $N_2$ and O. The secondary ionization effect of daytime photoelectron and several nighttime ionization sources are also considered in the model. The loss rates of ions include chemical reaction losses and ion recombination losses. In the model 20 chemical reactions are considered. A detailed description of chemical reactions and their reaction coefficient and collision frequencies can be found in the work of *Lei et al.* [2004a].

[12] In this model the differences between the temperatures of different ions are ignored. We only calculate the $O^+$ temperature. The heating source for electrons considered includes photoelectron heating, elastic collision with neutral particles ($N_2$, $O_2$ and O), vibrational and rotational excitation of $N_2$ and $O_2$, excitation of the fine structure levels of atomic oxygen, excitation from 3P to 1D state for atomic oxygen, and the energy transfer by electron-ion collisions; for the $O^+$, ion-electron collisions, ion-ion collisions and elastic and inelastic collisions with the neutrals are considered. For the lower boundary, $O^+$ temperature equals to neutral temperature and electron's temperature is obtained under the heat equilibrium assumption. The energy equations of electron and $O^+$ are solved by the same finite difference method as that of mass continuity equation [*Lei*, 2005]. The reader is referred to the paper of *Lei* [2005] for detailed description of above mentioned heating rates. The photoelectron heating effect is similar to that of *Millward* [1993].

[13] The neutral temperature and densities are taken from the NRLMSIS-00 model [*Picone et al.*, 2002], and NO concentration is calculated from an empirical model developed by *Titheridge* [1997]. The neutral winds are determined by the HWM-93 model [*Hedin et al.*, 1996]. The previous measurements and modeling studies [e.g., *Roble et al.*, 1986; *Salah et al.*, 1986; *Müller-Wodarg et al.*, 1998; *Korenkov et al.*, 2002; *Tomás et al.*, 2007] showed that during most of the eclipses events there is a slight change in the exospheric temperature and also a slight change in neutral concentration. In this study, we do not consider the possible effects of solar eclipse on neutral atmospheric compositions and temperature as well as neutral wind velocities. By our test, the model is steady and credible, and can reproduce most large-scale features of the ionosphere [*Yue et al.*, 2008a]. It is validated by the observational system data assimilation experiment and comparisons with several empirical models and observations [*Yue et al.*, 2008a, 2008b].

[14] To model the eclipse effects, the spectrum of solar radiation is multiplied by an eclipse factor *F*, a function of universal time, altitude, geographic longitude, and geographic latitude during the eclipse. The eclipse factor *F* is directly proportional to the unmasked fraction of the area of the Sun's photosphere. For any solar eclipse event, the unmasked fraction at a given location and time can be calculated by a JavaScript Eclipse Calculator which is a java

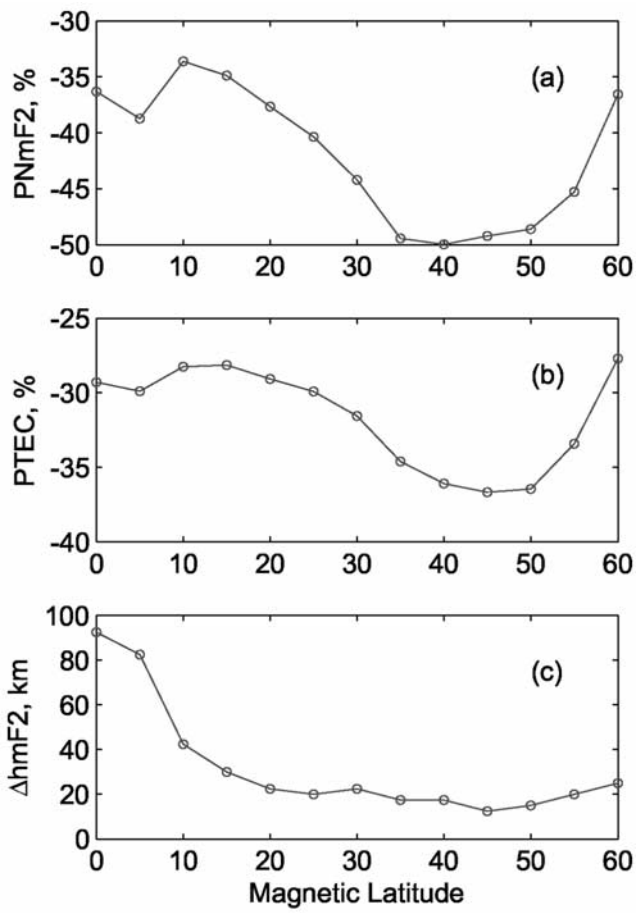


**Figure 2.** Latitudinal dependencies of simulated eclipse effects on (a) NmF2, (b) TEC, and (c) hmF2. For each simulation with the total eclipse occurring at a magnetic latitude of 5 × I-5 degrees (I = 1, 2, 3 . . . 13), the largest value of |PNmF2| and |PTEC| and the largest value of ΔhmF2 during the eclipse are chosen to describe the eclipse effect at this latitude.

program developed by Chris O'Byrne and Stephen McCann with the open source code on the web site (http://www.chris.obyrne.com/Eclipses/calculator.html). A detailed description of the eclipse factor *F* can be found in the work of *Le et al.* [2008a, 2008b].

[15] In this study, to model the latitudinal dependence of solar eclipse effects on the ionosphere we run the model with the total solar eclipse occurring at thirteen latitude regions from 0°N to 60°N at intervals of 5°, respectively. First, according to the method described above we calculated the variations in solar radiation at different latitudes of the longitudinal 90°W plane during the 26 February 1998 total solar eclipse. At this longitudinal plane, the total eclipse occurred at 0°N and the partial eclipse occurred in the regions from about 30°S to 40°N. Secondly, we move the entire eclipse region northward 5°, 10°, 15° . . ., 60° to make the total eclipse occur at other twelve latitude regions, respectively. In addition, all the simulations are carried out over the longitudinal 0°E plane with a time step of 60 seconds. The solar activity index is set as F10.7 = 140 and the magnetic activity index is set as Ap = 5. To examine the electrodynamics effect on the low-latitude eclipse effect more clearly, we made the total eclipse begin at around 9 LT (local time), reach the maximum obscuration at ∼10.5 LT, and end at ∼12 LT because the daytime vertical drifts have largest amplitudes during this period [*Scherliess and Fejer*, 1999]. In order to identify the solar eclipse effects on the ionosphere, one additional simulation excluding the eclipse shadow was run and the results are considered as the background level on the reference day. The percentage changes in Ne, NmF2 and TEC between the eclipse and noneclipse simulation are calculated, which are noted as PNe, PNmF2, and PTEC, respectively. The deviation of peak height of F2 layer on the eclipse day from that on the reference day is also calculated, which is noted as ΔhmF2. Besides the large response of electron density, electron temperature (Te) also has significant response to solar eclipses because of the reduction in photoelectron heating [*Evans*, 1965a; *Salah et al.*, 1986; *Roble et al.*, 1986; *Boitman et al.*, 1999]. So the deviation of electron temperature on the eclipse day from that on the reference day, ΔTe, is also calculated.

## 4. Model Results and Analysis

[16] For each simulation with the total eclipse occurring at magnetic latitude of 5 × I-5 degrees (I = 1, 2, 3 . . . 13), the largest percentage decreases in NmF2 (largest |PNmF2|) and in TEC (largest |PTEC|) and the largest increase in hmF2 during the eclipse are chosen to describe the eclipse effect at this latitude, and are plotted in Figures 2a, 2b, and 2c, respectively. From Figure 2, one can see that for the eclipse effects on NmF2 and TEC, there are four distinct features: the largest effect is at middle latitude of about 40 degrees; the effect at low latitudes (0°–25°) is smaller than that at middle latitudes (30°–50°); the effect at the EIA region (10°–20°) is slightly smaller than that at the magnetic equator (0°–5°); for the latitudes larger than 40°, the effect decreases with increasing latitude. Comparing the experimental data in Figure 1 to the simulations in Figure 2, one can see that the principal latitudinal variation trend of the experimental data is similar to that of the simulations, but there are also some differences: for the experimental data the largest eclipse effect on NmF2 and TEC both occur at latitude of ∼30°, whereas it appears at latitudes of ∼40° and ∼45° for the simulated NmF2 and TEC, respectively. For the eclipse effects on hmF2, one can see that the largest uplift in hmF2 occurs at the magnetic equator, which reaches nearly 100 km; the uplift decreases steeply with increasing latitude from ΔhmF2 ≈ 100 km at the magnetic equator to ΔhmF2 ≈ 20 km at middle latitudes. Furthermore, the simulated results show that there would be a decrease in hmF2 after the end of the eclipse and the decrease amplitude also decreases with latitude from about 50 km at the equator to less than10 km at the middle latitude. These simulated results are in agreement with the previous measurements. Previous experimental observations have shown that during a solar eclipse there is a slight increase of about 20 km in the F2 layer virtual height (or F2 layer peak height) at middle latitudes at some time after the totality when the F2 layer critical frequency dropped to the smallest value [e.g., *Cohen*, 1984; *Boitman et al.*, 1999; *MacPherson et al.*, 2000; *Afraimovich et al.*, 2002; *Farges*

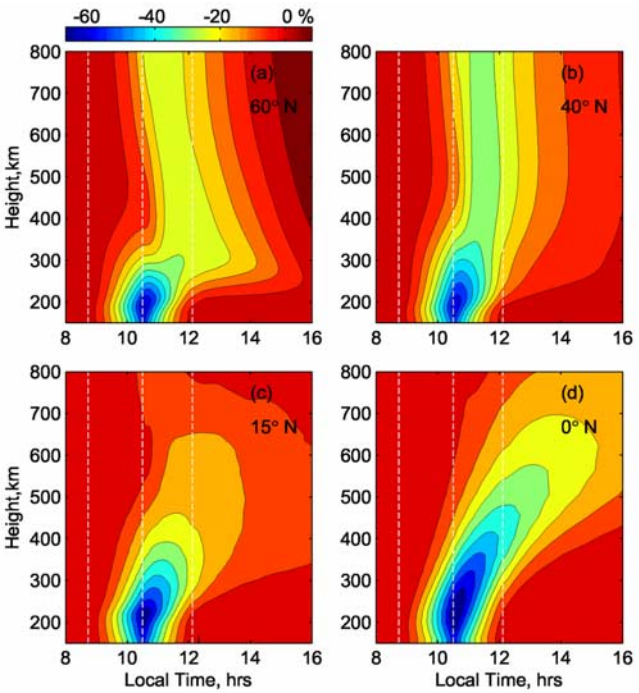


**Figure 3.** Spatial and temporal evolutions of the simulated PNe over (a) mid-high latitude 60°N, (b) middle latitude 40°N, (c) EIA region 15°N, and (d) equator 0°N when the total eclipse occurred at the corresponding locations, respectively. The three dashed lines indicate the beginning, totality, and end of the eclipse, respectively.

*et al.*, 2003]. Some simulated studies also show such an increase in F2 layer peak height at middle latitude eclipses [*Stubbe*, 1970; *Boitman et al.*, 1999; *Le et al.*, 2008a, 2008b]. However, at low latitudes especially at the magnetic equator, there is much larger increase in the F2 layer virtual height [*Sridharan et al.*, 2002; *Adeniyi et al.*, 2007].

[17] As shown in Figures 1 and 2, both the measurements and the simulated results show that eclipse effects on the ionosphere have obvious latitudinal dependence, which can be approximately separated into four types, namely, eclipse effects in the magnetic equator region, EIA region, middle latitude, and mid-high latitude, respectively. The latitudes of 60°N, 40°N, 15°N, and 0°N, are considered as the representations of mid-high latitude, middle latitude, EIA region, and equatorial region, respectively. Figure 3 illustrates the spatial and temporal evolutions of PNe over mid-high latitude (60°N), middle latitude (40°N), EIA region (15°N), and equatorial region (0°N) with the total eclipse occurring at the corresponding locations, respectively. From Figure 3, we can see that the eclipse effects below 200 km have no latitudinal difference. The largest percentage decrease in Ne occurs at about 200 km for the eclipses at all the latitude region. Furthermore, the temporal variation of PNe at low altitudes below 200 km is almost synchronous with that of the solar EUV radiation induced by solar eclipse. As is known, the ionospheric behavior at low altitudes (the E and F1 regions) at all the latitudes is governed by photochemical processes, so the decrease of solar radiation during a solar eclipse leads to the decrease in electron production rate and electron density and the time delay of the Ne response does not exceed 2 min because of the very small time constant of loss.

[18] In contrast to the results at the low altitudes, Figure 3 shows distinct latitudinal differences in the eclipse effect on the electron density at high altitudes. When looking at Figure 3, one can see that the eclipse effect on the middle latitudes (mid-high latitude 60°N also included) is quite different from that on the low latitudes (including 15°N and 0°N). Figures 3a and 3b show that for middle latitudes, there are almost identical electron density responses at high altitudes of about 300 km and above. There is a large reduction in Ne of about 30–35% and a large time delay of nearly one hour between totality and the largest reduction of Ne. The F2 layer at middle latitudes is thought to be largely controlled by plasma diffusion which determines the height hmF2 at which the F2 peak is found. Theoretically, diffusion tends to smooth out differences in the behavior of the layer at different heights and this 'equalizing' effect of diffusion would also cause the similar electron density responses at all heights in the top F2 layer [*Rishbeth*, 1968]. There are also some differences between the Ne responses at 60°N and those at 40°N. The amplitude of the reduction in Ne over the entire altitudes of about 200 km and above is smaller at 60°N than at 40°N, on the other hand, the electron density responses at the heights of 250–400 km at 60°N are much delayed and have the longer duration. These differences between 60°N and 40°N should be related to the dip angle effect that the larger dip angle causes the larger downward diffusion flux which makes up the ion losses in the F region. That is, compared to middle latitude of 40°N, the smaller percentage reduction of NmF2 and TEC at mid-high latitude of 60°N is attributed to the larger downward diffusion from top ionosphere because of the larger dip angle. The detailed discussion about the dip angle effect in middle latitudes is in the next section.

[19] For the eclipse effect on Ne at low latitudes, one can see from Figures 3c and 3d that the largest reduction of electron density decreases rapidly upward at low latitudes because of the increase of the time constant for loss. Since diffusion only takes place along magnetic field lines, the near horizontal diffusion at low latitudes cannot smooth out the eclipse effects at different heights as it does at middle latitudes. Figures 3c and 3d also show that the time delay between totality and the greatest reduction of Ne also rapidly increases upwards, which causes the height of the largest percentage decrease in Ne rising continually with time. These simulated results seem to show that the decrease in electron density in the F region starts from the lower heights of the region and progress upward with time. This feature should result from the E × B vertical drift. There are also some difference between the Ne response at 15°N and those at 0°N. The eclipse effect on the Ne at 300 km and above is much smaller at 15°N than at 0°N. For example, the magnitude of largest decrease in Ne at 1200LT is −23.5% at ∼360 km at 15°N, while it reaches −39% at ∼405 km at 0°N. The detailed discussion about these feature in low latitudes is in the next section.

[20] Comparing the results at middle latitudes as shown in Figure 3b with the results at low latitudes as shown in Figures 3c and 3d, one can see that for the same height below 400 km, the electron density response is larger at low latitudes. It should be noted that the hmF2 values at 40°N,

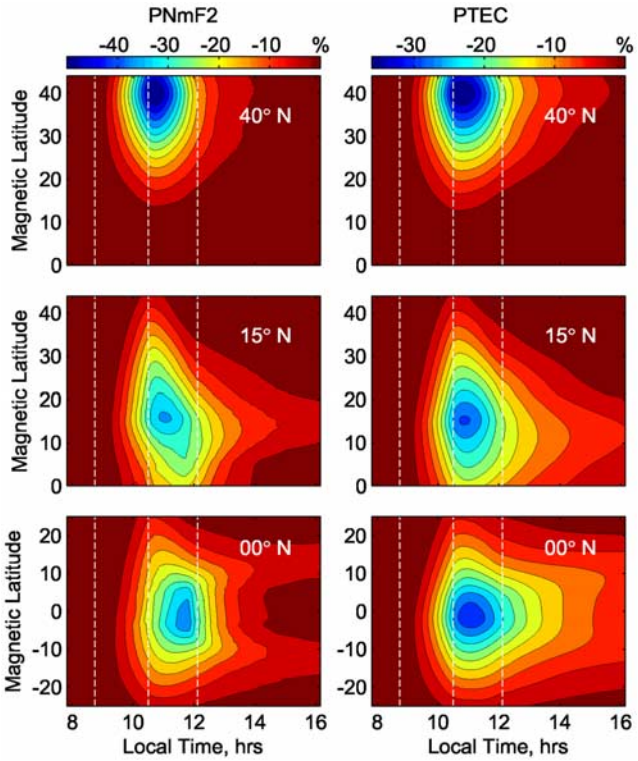


**Figure 4.** Temporal evolutions of the simulated PNmF2 and PTEC when the total eclipse occurred at middle latitude (40°N), EIA region (15°N), and equatorial region (0°N), respectively. The three dashed lines indicate the beginning, totality, and end of the eclipse, respectively.

15°N, and 0°N at ~1030 LT on the reference day are ~245 km, ~310 km, and ~375 km, respectively. That is, because of the E × B vertical drift effect the hmF2 values at low latitudes are much larger than those at middle latitudes. Thus although there is the larger electron density response at low heights at low latitudes, the NmF2 responses are still much smaller than those at middle latitudes because of the much higher location of hmF2 at low latitudes and the electron density response decreasing rapidly with increasing height. Additionally, the smaller electron density reduction at the heights near hmF2 and above in low latitudes would also cause the smaller TEC reduction in this region.

[21] Figure 4 illustrates the temporal evolutions of the simulated PNmF2 and PTEC when the total eclipse occurred at middle latitude (40°N), EIA region (15°N), and equatorial region (0°N), respectively. The temporal evolution of the simulated PNmF2 and PTEC at 60°N is similar to that at 40°N, so it is not plotted in Figure 4. From Figure 4, one can see that the percentage decreases in NmF2 and TEC are larger at middle latitude than at low latitude but the durations of NmF2 and TEC responses are longer at low latitude than at middle latitude. Furthermore, the duration is longest in the EIA region even though the total eclipse occurred at equatorial region. Figure 4 also shows that the time delay of NmF2 responses is longest (about 70 min) at equatorial region and shortest (about 13 min) at middle latitude and the time delay of TEC responses also is longest (about 36 min) at equatorial region and shortest (about 13 min) at middle latitude. For the similar event of the total solar eclipse on 29 March 2006, *Adeniyi et al.* [2007] reported a time delay of foF2 response of around 40 min at low latitude and *Afraimovich et al.* [2007] reported a time delay of TEC response of about 11 min at middle latitude. Our simulated results are in agreement with these measurements. Comparing the NmF2 response with the TEC response, we find that the duration of TEC response is much longer than that of NmF2 response for all the latitude regions. TEC is the integration of electron density of the entire heights. As shown in Figure 3, before the totality there is the much larger electron density response at low altitudes than at high altitudes, thus the contribution of TEC response is mostly from the electron density response at the low altitudes; while after the totality the electron density response is largely from high altitudes. The contribution of TEC response from high altitudes is more than that from low altitudes. In addition, there is a long duration in the electron density response at high altitudes because of the large time constant there. Therefore the long duration of the electron density response at high altitudes and the initial contribution from lower altitudes should be responsible for the long duration of TEC response.

[22] Besides the large response of electron density, electron temperature also has significant response to solar eclipses because of the reduction in photoelectron heating. Figure 5 illustrates the spatial and temporal evolutions of ΔTe over mid-high latitude (60°N), middle latitude (40°N), EIA region (15°N), and equatorial region (0°N) with the total eclipse occurring at the corresponding places, respectively. Figure 5 shows that there is distinct latitudinal difference in the eclipse effect on the electron temperature. The variation in Te at middle latitudes (mid-high latitude 60°N also included) is quite different from that at low latitudes (including 15°N and 0°N). For variations in

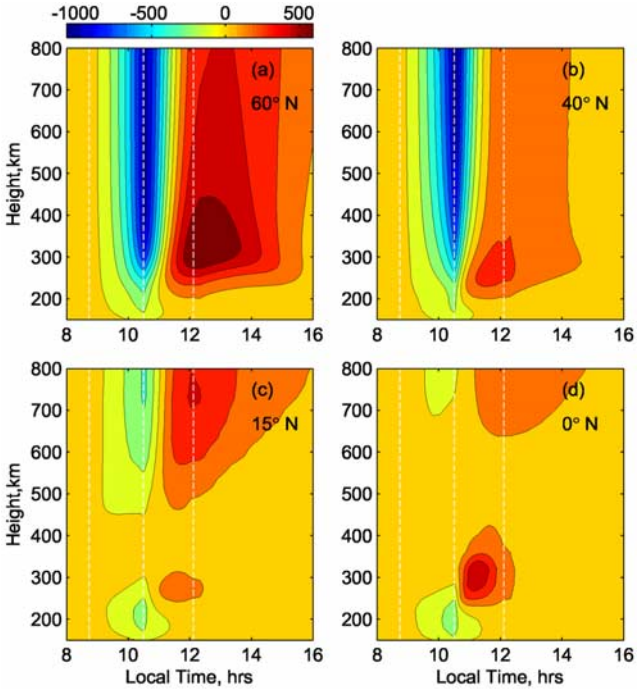


**Figure 5.** Same as Figure 3 but for ΔTe.

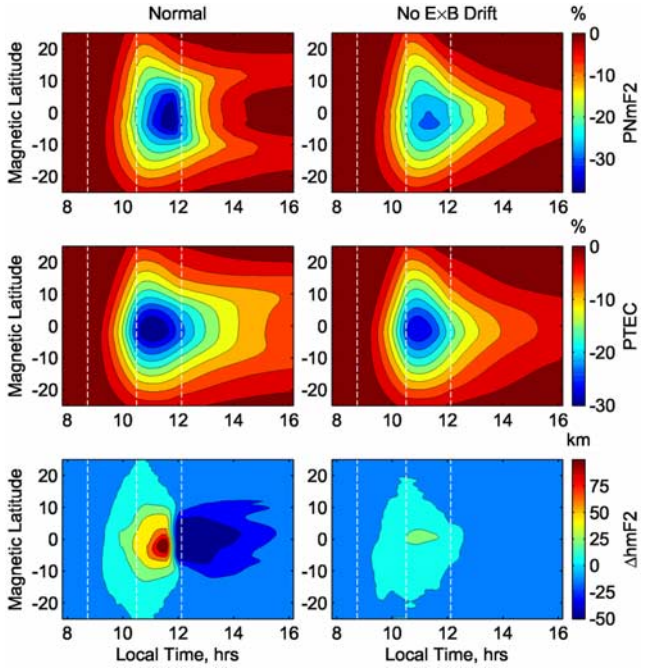


**Figure 6.** Eclipse effects on the NmF2, TEC, and hmF2 when the eclipse occurred at the magnetic equator. The left indicates the results with the normal condition and the right indicates the results with the E × B vertical drift not considered during the eclipse. The three dashed lines indicate the beginning, totality, and end of the eclipse, respectively.

electron temperature at middle latitudes, Figures 5a and 5b show that the beginning of the eclipse occurs simultaneously with an overall decrease in electron temperature throughout the entire height range. At all heights changes in electron temperature are synchronous with the eclipse magnitude. The largest drop of electron temperature occurs at the time of totality. Similar results were reported previously [e.g., *Evans*, 1965a; *Salah et al.*, 1986; *Roble et al.*, 1986; *Boitman et al.*, 1999; *Le et al.*, 2008a]. However, compared to the changes at middle latitudes, the electron temperature response at low latitudes is much smaller, especially for high altitudes above 300 km. Furthermore, the electron temperature response is very small at the heights of 300–450 km for 15°N and at the heights of 400–600 km for 0°N. *Tomás et al.* [2007] also reported that no obvious change in electron temperature was found at ~370 km over magnetic equator by the CHAMP satellite during the solar eclipse of 8 April 2005. Similar results were reported by *Van Zandt et al.* [1960].

[23] As it is well known that most of the photoelectrons are produced at low heights below 300 km, some of them are consumed by heating the local ionosphere gas and others can propagate along the magnetic field lines to heat the gas at higher heights or even travel to the conjugate hemisphere. That is, the photoelectron heat at high heights mainly comes from the photoelectrons produced at the conjugate low heights along the magnetic field line. For the middle latitude region, there is very small difference of latitude value between the high height and its conjugate low height because of the large dip angle. Thus when a total eclipse occurred at middle latitude, there would be a large decrease in electron temperature at high heights because of the large reduction of photoelectron production rate at the conjugate low heights. However, for the low-latitude region, there is large difference of latitude value between the high height and its conjugate low height because of the small dip angle. For example, for a high height of 800 km above magnetic equator, its conjugate low height of 300 km is locates at about 18°N. Therefore when a total eclipse occurred at low latitude, there would be much smaller decrease in electron temperature at high heights because of the much smaller reduction of photoelectron production rate at the conjugate low heights where only a partial eclipse with small eclipse magnitude occurring.

## 5. Discussion

### 5.1. E × B Vertical Drift Effect

[24] Both the measurements and simulated results show that the ionospheric responses to solar eclipses at low latitudes are much different from those at middle latitudes. As it is well known, the fountain effect driven by the E × B vertical plasma drift is one of the most important dynamics processes for the behavior of the ionosphere in the low latitude. During the solar eclipses, this E × B vertical drift also has significant effect on the ionospheric responses in the low latitude including the magnetic equator and the EIA region [*Cheng et al.*, 1992; *Tsai and Liu*, 1999; *Sridharan et al.*, 2002; *Tomás et al.*, 2007; *Adeniyi et al.*, 2007]. *Cheng et al.* [1992] and *Tsai and Liu* [1999] suggested the fountain effect is essential for the ionospheric behavior during the solar eclipses. In the study of *Sridharan et al.* [2002], the large rise in the F layer virtual height was ascribed to the enhanced post sunset vertical drift caused by the larger F region dynamo effect caused by the sudden removal of the E region loading during the solar eclipse. The measurements from the CHAMP satellite during the 8 April 2005 solar eclipse also show that the plasma fountain at the equator was strongly enhanced during this eclipse [*Tomás et al.*, 2007].

[25] In this study, to further investigate the fountain effect on the behavior of the ionosphere at low latitude during a solar eclipse we run the simulation again with the total eclipse occurring at the magnetic equator but the E × B vertical drift is not considered during the solar eclipse. Figure 6 illustrates the eclipse effects on the NmF2, TEC, and hmF2 when the eclipse occurred at the magnetic equator. The left indicates the simulated results with normal condition and the right indicates the simulated results with the E × B vertical drift not considered during the eclipse. From Figure 6, one can see that one of the most significant differences between these two simulations is the much smaller hmF2 response when the E × B vertical drift is not considered. That is, the large rise in the hmF2 at equator during the solar eclipse is mainly driven by the vertical drift. Figure 6 also shows that if the E × B vertical drift is not considered during the eclipse, the amplitudes of decrease in NmF2 and TEC at the equator would be much smaller and the duration of the eclipse effect in the EIA region on NmF2 and TEC would be much less. Figure 7 shows the eclipse effect on Ne at different heights when E × B drift was considered and when E × B drift not considered, respec-

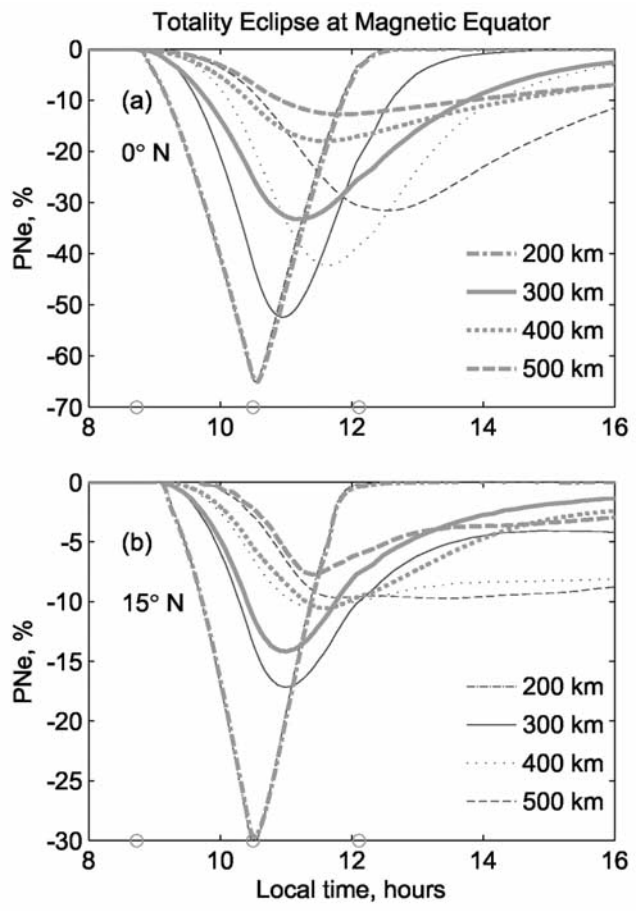


**Figure 7.** Temporal variation of the PNe at various height at (a) magnetic equator (0°N) and (b) EIA region (15°N) when a total eclipse occurred at the equator. The bold lines indicate the results with E × B drift considered, and the thin lines indicate the results with E × B not considered. The circles in the *x* axis indicate the beginning, totality, and end of the eclipse.

tively. The results show that the low height of 200 km is not affected at all. However, the eclipse effects at higher heights would decrease a lot if the vertical drift is not considered. Figure 7b also show that when the vertical drift is considered, even after the end of the eclipse the electron densities at high heights of 400 km and 500 km in the EIA region do not recover with time but keep a decrease of ∼10% for several hours.

[26] Figure 8 illustrates the evolutions of absolute change in Ne from 0930 LT to 1500 LT when a total solar eclipse occurred at the magnetic equator. The time the eclipse began, when totality occurred, and when the eclipse ended are ∼0900 LT, 1030 LT, and 1200 LT, respectively. From Figure 8, we can see that the height of the largest decrease in Ne rises with time successively from the initial stage of the eclipse to several hours after the end of the eclipse and the velocity of this uplift is much larger after the totality (from ∼284 km at 1030 LT to ∼474 km at 1400 LT) than before the totality (from ∼250 km at 0930 LT to ∼284 km at 1030 LT). Before the totality, the uplift mainly caused by the vertical drift. However, after the totality, the electron production rate increases gradually with time at all altitudes and the electron density response to the increase of electron production rate is faster at lower altitudes. The upward drift of ionization coupled with the recovery of the electron production cause the larger uplift of the height of largest decrease in Ne. The decrease in electron densities at altitudes below the hmF2 is much larger than that at latitudes above the hmF2, which would cause the great change in the shape of the height profile of the electron density and result in the large rise of the hmF2 like the peak increase in hmF2 of around 100 km at ∼1130 LT as shown in Figure 6. On the contrary, if there is much larger decrease in electron density at altitudes above hmF2 than at altitudes below hmF2, the shape of the height profile of the electron density would be greatly changed and there will be a great drop in the location of the hmF2. For example, there is a large decrease of around 50 km around 1210 LT as shown in Figure 6.

[27] Figure 8 also shows that the eclipse effect at low latitude can be gradually transmitted through the fountain effect to the EIA region. The evident feature of this transmission can be found at 14 LT and especially at 15 LT with two principal decrease at around 460 km at latitude ±10°. The long duration of the eclipse effect at high heights in the EIA region (as shown in Figure 7b) should be ascribed to this transmission from the equatorial region. Compared to the values on the reference day, the plasma diffusing to the EIA region from the equatorial region through the fountain effect would be smaller during the eclipse because of the large decrease in Ne in the equatorial

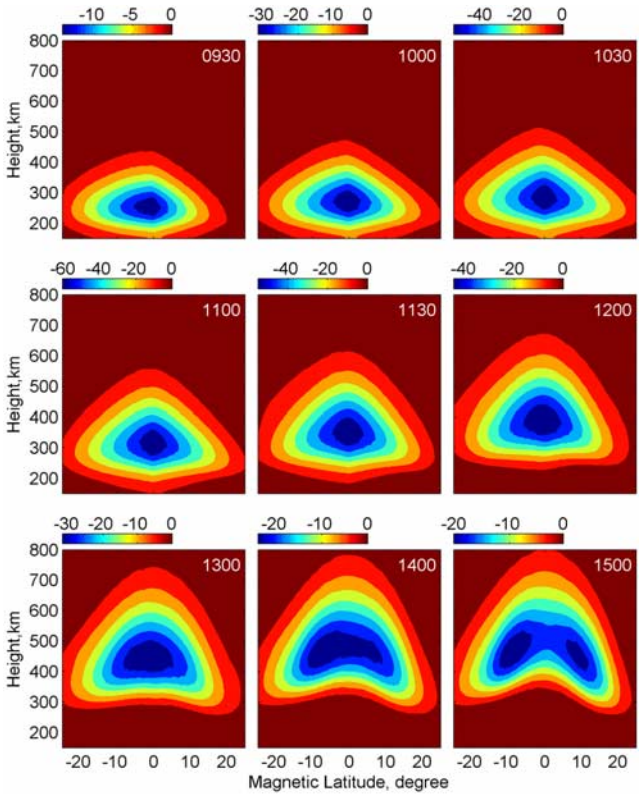


**Figure 8.** The evolutions of absolute change in Ne (in unit of $10^{10}$ el/m$^3$) from 0930 LT to 1500 LT when a solar eclipse occurred at the magnetic equator. The text in each panel indicates the local time.

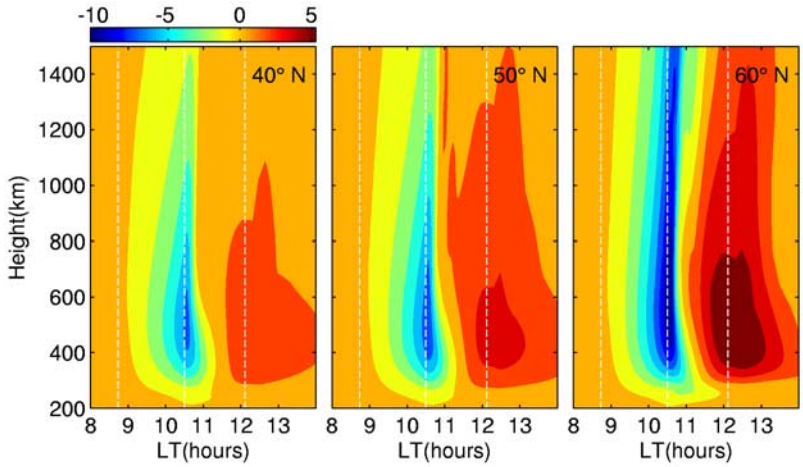


**Figure 9.** Plasma flux at 40°N, 50°N, and 60°N when the total eclipse occurred at 40°N, 50°N, and 60°N, respectively. It is in unit of $10^{12}$ $m^{-2}$ $s^{-1}$. The three dashed lines indicate the begin, totality, and end of the eclipse, respectively. The positive (negative) values indicate the upward (downward) diffusions.

region. The plasma diffusing to the EIA region from the equatorial region would not decrease immediately when the Ne in the equatorial region decreased because the plasma diffusion process from the equatorial region to the EIA region need several hours. So as shown in Figure 7b, even after the end of the eclipse the electron densities at high heights of 400 km and 500 km in the EIA region do not recover with time but keep a decrease of ~10% for several hours.

[28] The discussion above shows that the equatorial ionosphere responses to a solar eclipse would be significantly affected by the E × B vertical drift because the large depletion of electron at low altitudes can be transmitted to high altitudes through the plasma vertical drift. Furthermore, the depression in Ne in the equatorial region also will be transmitted to the EIA region through the fountain effect and affect the eclipse effect in this region.

### 5.2. Dip Angle Effect

[29] Both the measurements and simulated results (as shown in Figures 1 and 3) show that for the eclipse effects in the mid-high latitudes, the depressions of NmF2 and TEC are smaller at higher latitudes. Figure 9 illustrates the plasma flux at 40°N, 50°N, and 60°N when the total eclipse occurred at 40°N, 50°N, and 60°N, respectively. The magnetic dip angles at these locations are 55 degrees, 64 degrees, and 72 degrees, respectively. The positive (negative) values indicate the upward (downward) diffussions. From Figure 9, one can see that for all the three latitudes there is the strongest downward plasma flux at the totality and then the downward plasma flux gradually decreases with time and reverse at some time before the end of eclipse. At middle latitudes the eclipse can cause a rapid lowering of electron temperature (as shown in Figure 5) and a subsequent change in the diffusive equilibrium-scale height; therefore it results in ionizations moving downward from the plasmasphere. The downward ionization flux will make up for electron losses at low heights. There are many measurements and computer simulations on such an eclipse effect in the past [*Evans*, 1965b; *Stubbe*, 1970; *Salah et al.*, 1986; *Boitman et al.*, 1999; *Le et al.*, 2008a]. A look at Figure 9 shows an evident feature of larger downward plasma flux at the high latitude with the larger dip angle. As is well known, the effect of the dip ($I$) is to control the rate of diffusion according to $\sin^2 I$. So the larger dip causes the larger downward diffusion flux. The larger downward diffusion flux would alleviate the depression of electron density of F region by the larger amplitude, which results in the smaller eclipse effect at the F region heights (as shown in Figure 2).

[30] To better understand the role of the change in temperature and the role of dip angle, we carried out three simulations again at these three latitudes by running the model with no change in plasma temperature during the solar eclipses. The simulated results show almost the same ionospheric response in these three simulations. Also, there is small difference in ionization flux between the control day and the eclipse day in these simulations because there is no change in plasma temperature. Early in 1960s, *Evans* [1965b] ascribed the increase in foF2 at three ionosonde stations during the 20 July 1963 total solar eclipse to the large downward plasma diffusion flux from the top ionosphere because of the large magnetic dip angles at these stations. Additionally, using the similar method as this study, we have studied the dip angle effect in another paper [*Le et al.*, 2008b] and obtained the same conclusion that the larger dip angle would cause the larger downward diffusion flux which makes up the plasma losses in the F region and subsequently results in the smaller changes in electron concentration in this region.

## 6. Summary

[31] In this study, we statistically analyzed the latitudinal dependence of F2 layer peak electron densities and total electron content (TEC) responses to solar eclipses by using the NmF2 data from the ionosonde observations during fifteen eclipse events from the year of 1973 to 2006 and the GPS TEC observations during six solar eclipse events from the year of 1999 to 2006. The observed results show that the NmF2 and TEC responses have the same latitudinal dependence: the largest response is at middle latitude of about

40 degrees; the response at low latitudes is smaller than that at middle latitudes; for the latitudes larger than 40 degrees, the response decreases with increasing latitude.

[32] We carried out a series of simulations by using a theoretical ionospheric model to study the latitudinal dependence of solar eclipse effects on the ionosphere. To model this latitudinal dependence we run the model with the total solar eclipse occurring at thirteen latitude regions from 0°N to 60°N at intervals of 5°, respectively. All the simulations are carried out over the longitudinal 0°E plane. The simulated results show the similar latitudinal dependence of eclipse effect on NmF2 and TEC with the observations. The study suggested the following conclusions.

[33] 1. The electron density responses at low heights below 400 km are larger at low latitudes than at middle latitudes. However, the NmF2 responses at low latitudes are still much smaller than those at middle latitudes because of the much higher location of hmF2 at low latitudes and the electron density response decreasing rapidly with increasing height.

[34] 2. The decrease in electron temperature at high heights of 300 km and above is much smaller at low latitudes than at middle latitudes. For the low-latitude region, there is large difference of latitude value between the high height and its conjugate low height because of the small dip angle. When a total eclipse occurred at high heights of low latitudes, at its conjugate low heights only a partial eclipse with small eclipse magnitude occurred. Thus there would be much smaller decrease in electron temperature at high heights because of the much smaller reduction of photoelectron production rate at the conjugate low heights where only a partial eclipse occurring.

[35] 3. The equatorial ionosphere response to a solar eclipse would be significantly affected by the E × B vertical drift because the large depletion of electron at low altitudes can be transmitted to high altitudes through the plasma vertical drift. Then the large depression in Ne in the equatorial region would reduce the plasma diffusion flux reaching the EIA region along magnetic field line and hence affect the ionospheric response to the eclipse in the EIA region.

[36] 4. For the middle latitude ionosphere, the dip angle has a large effect on the ionospheric response to a solar eclipse. The larger dip would cause the larger downward diffusion flux which can partly make up for the plasma loss and alleviate the depression of electron density of F region. Therefore for the middle latitudes, the NmF2 and TEC responses to the solar eclipse decreases with increasing latitude.

[37] **Acknowledgments.** The authors acknowledge the Space Physics Interactive Data Resource of the National Geophysical Data Center and Data-sharing Network of Earth System Science in China for supplying the ionodonde data. The authors also thank the International GNSS Service (IGS) for providing GPS network data. This research was supported by the National Natural Science Foundation of China (40725014, 40674090, and 40636032) and the National Important Basic Research Project (2006CB806306).

[38] Zuyin Pu thanks Jacob Adeniyi and another reviewer for their assistance in evaluating this paper.

## References

Adeniyi, J. O., S. M. Radicella, I. A. Adimula, A. A. Willoughby, O. A. Oladipo, and O. Olawepo (2007), Signature of the 29 March 2006 eclipse on the ionosphere over an equatorial station, *J. Geophys. Res.*, *112*, A06314, doi:10.1029/2006JA012197.

Afraimovich, E. L., K. S. Palamartchouk, N. P. Perevalova, V. V. Chemukhov, A. V. Lukhnev, and V. T. Zalutsky (1998), Ionospheric effects of the solar eclipse of March 9, 1997, as deduced from GPS data, *Geophys. Res. Lett.*, *25*(4), 465–468.

Afraimovich, E. L., E. A. Kosogorov, and O. S. Lesyuta (2002), Effects of the August 11, 1999 total solar eclipse as deduced from total electron content measurements at the GPS network, *J. Atmos. Sol. Terr. Phys.*, *64*, 1933–1941.

Afraimovich, E. L., S. V. Voeykov, N. P. Perevalova, V. V. Vodyannikov, G. I. Gordienko, Yu. G. Litvinov, and A. F. Yakovets (2007), Ionospheric Effects of the March 29, 2006, solar eclipse over Kazakhstan, *Geomagn. Aeron.*, *47*(4), 461–469.

Boitman, O. N., A. D. Kalikhman, and A. V. Tashchilin (1999), The mid-latitude ionosphere during the total solar eclipse of March 9, 1997, *J. Geophys. Res.*, *104*(A12), 28,197–28,206.

Cheng, K., Y.-N. Huang, and S.-W. Chen (1992), Ionospheric effects of the solar eclipse of September 23, 1987, around the equatorial anomaly crest region, *J. Geophys. Res.*, *97*(A1), 103–111.

Cohen, E. A. (1984), The study of the effect of solar eclipses on the ionosphere based on satellite beacon observations, *Radio Sci.*, *19*(3), 769–777.

Davis, C. J., M. Lockwood, S. A. Bell, J. A. Smith, and E. M. Clarke (2000), Ionospheric measurements of relative coronal brightness during the total solar eclipses of 11 August, 1999 and 9 July, 1945, *Ann. Geophys.*, *18*, 182–190.

Davis, C. J., E. M. Clarke, R. A. Bamford, M. Lockwood, and S. A. Bell (2001), Long term changes in EUV and X-ray emissions from the solar corona and chromosphere as measured by the response of the Earth's ionosphere during total solar eclipses from 1932 to 1999, *Ann. Geophys.*, *19*, 263–273.

Evans, J. V. (1965a), An F region eclipse, *J. Geophys. Res.*, *70*(1), 131–142.

Evans, J. V. (1965b), On the behavior of foF2 during solar eclipses, *J. Geophys. Res.*, *70*(3), 733–738.

Farges, T., J. C. Jodogne, R. Bamford, Y. Le Roux, F. Gauthier, P. M. Vila, D. Altadill, J. G. Sole, and G. Miro (2001), Disturbances of the western European ionosphere during the total solar eclipse of 11 August 1999 measured by a wide ionosonde and radar network, *J. Atmos. Sol. Terr. Phys.*, *63*, 915–924.

Farges, T., A. Le Pichon, E. Blanc, S. Perez, and B. Alcoverro (2003), Response of the lower atmosphere and the ionosphere to the eclipse of August 11, 1999, *J. Atmos. Sol. Terr. Phys.*, *65*, 717–726.

Hedin, A. E., et al. (1996), Empirical wind model for the upper, middle and lower atmosphere, *J. Atmos. Terr. Phys.*, *58*, 1421–1447.

Hunter, A. N., B. K. Holman, D. G. Fieldgate, and R. Kelleher (1974), Faraday rotation studies in Africa during the solar eclipse of June 30, 1973, *Nature*, *250*, 205–206.

Klobuchar, J. A., and H. E. Whitney (1965), Ionospheric electron content measurements during a solar eclipse, *J. Geophys. Res.*, *70*(5), 1254–1257.

Korenkov, Y. N., V. V. Klimenko, F. S. Bessarab, N. S. Nutsvalyan, and I. Stanislawska (2002), Model/data comparison of the F2-region parameters for the 11 August 1999 solar eclipse, *Adv. Space Res.*, *31*(4), 995–1000.

Le, H., L. Liu, X. Yue, and W. Wan (2008a), The ionospheric responses to the 11 August 1999 solar eclipse: Observations and modeling, *Ann. Geophys.*, *26*, 107–116.

Le, H., L. Liu, X. Yue, and W. Wan (2008b), The mid-latitude F2 layer during solar eclipses: Observations and modeling, *J. Geophys. Res.*, *113*, A08309, doi:10.1029/2007JA013012.

Le, H., L. Liu, X. Yue, and W. Wan (2009), The ionospheric behavior in conjugate hemispheres during the 3 October 2005 solar eclipse, *Ann. Geophys.*, *27*, 179–184.

Lei, J. (2005), Statistical analysis and modeling investigation of middle latitude ionosphere, dissertation for the doctoral degree, pp. 1–121, Inst. of Geol. and Geophys., Chinese Acad. of Sciences, Beijing, China.

Lei, J., L. Liu, W. Wan, and S. R. Zhang (2004a), Modeling the behavior of ionosphere above Millstone Hill during the September 21–27, 1998 storm, *J. Atmos. Sol. Terr. Phys.*, *66*, 1093–1102.

Lei, J., L. Liu, W. Wan, and S. R. Zhang (2004b), Model results for the ionospheric lower transition height over mid-latitude, *Ann. Geophys.*, *22*, 2037–2045.

Liu, L., W. Wan, J. N. Tu, Z. T. Bao, and C. K. Yeh (1999), Modeling study of the ionospheric effects during a total solar eclipse, *Chin. J. Geophys.*, *42*(3), 296–302.

MacPherson, B., S. A. González, M. P. Sulzer, G. J. Bailey, F. Djuth, and P. Rodriguez (2000), Measurements of the topside ionosphere over Arecibo during the total solar eclipse of February 26, 1998, *J. Geophys. Res.*, *105*(A10), 23,055–23,067.

Millward, G. H. (1993), A global model of the Earth's thermosphere, ionosphere and plasmasphere: Theoretical studies of the response to enhanced high-latitude convection, dissertation for the doctoral degree, pp. 1–195, Univ. of Sheffield, Sheffield, U. K.

Müller-Wodarg, I. C. F., A. D. Aylward, and M. Lockwood (1998), Effects of a mid-latitude solar eclipse on the thermosphere and ionosphere—A modelling study, *Geophys. Res. Lett.*, *25*(20), 3787–3790.

Oliver, W. L., and S. A. Bowhill (1974), The F1 region during a solar eclipse, *Radio Sci.*, *9*(2), 185–195.

Picone, J. M., A. E. Hedin, D. P. Drob, and A. C. Aikin (2002), NRLMSISE-00 empirical model of the atmosphere: Statistical comparisons and scientific issues, *J. Geophys. Res.*, *107*(A12), 1468, doi:10.1029/2002JA009430.

Richards, P. G., J. A. Fennelly, and D. G. Torr (1994), EUVAC: A solar EUV flux model for aeronomic calculations, *J. Geophys. Res.*, *99*, 8981–8992.

Rishbeth, H. (1968), Solar eclipses and ionospheric theory, *Space Sci. Rev.*, *8*(4), 543–554.

Roble, R. G., B. A. Emery, and E. C. Ridley (1986), Ionospheric and thermospheric response over Millstone Hill to the May 30, 1984, annular solar eclipse, *J. Geophys. Res.*, *91*(A2), 1661–1670.

Salah, J. E., W. L. Oliver, J. C. Foster, J. M. Holt, B. Emery, and R. Roble (1986), Observations of the May 30, 1984, annular solar eclipse at Millstone Hill, *J. Geophys. Res.*, *91*(A2), 1651–1660.

Scherliess, L., and B. G. Fejer (1999), Radar and satellite global equatorial F region vertical drift model, *J. Geophys. Res.*, *104*(A4), 6829–6842.

Sridharan, R., C. V. Devasia, N. Jyoti, D. Tiwari, K. S. Viswanathan, and K. S. V. Subbarao (2002), Effects of solar eclipse on the electrodynamical processes of the equatorial ionosphere: A case study during 11 August 1999 dusk time total solar eclipse over India, *Ann. Geophys.*, *20*, 1977–1985.

Stubbe, P. (1970), The F-region during an eclipse—A theoretical study, *J. Geophys. Res.*, *32*, 1109–1116.

Titheridge, J. E. (1997), Model results for the ionospheric E-region: Solar and seasonal changes, *Ann. Geophys.*, *15*, 63–78.

Tomás, A. T., H. Lühr, M. Förster, S. Rentz, and M. Rother (2007), Observations of the low-latitude solar eclipse on 8 April 2005 by CHAMP, *J. Geophys. Res.*, *112*, A06303, doi:10.1029/2006JA012168.

Tsai, H. F., and J. Y. Liu (1999), Ionospheric total electron content response to solar eclipses, *J. Geophys. Res.*, *104*(A6), 12,657–12,668.

Tu, J. N., L. Liu, and Z. T. Bao (1997), An low latitude theoretical ionospheric model (in Chinese), *Chinese J. Space Sci.*, *17*, 212–219.

Van Zandt, T. E., R. B. Norton, and G. H. Stonehocker (1960), Photochemical rates in the equatorial F2 region from the 1958 eclipse, *J. Geophys. Res.*, *65*(7), 2003–2009.

Yue, X., W. Wan, L. Liu, H. Le, Y. Chen, and T. Yu (2008a), Development of a middle and low latitude theoretical ionospheric model and an observation system data assimilation experiment, *Chin. Sci. Bull.*, *53*(1), 94–101.

Yue, X., W. Wan, L. Liu, B. Ning, B. Zhao, and M. Zhang (2008b), TIME-IGGCAS model validation: Comparisons with empirical models and observations, *Sci. China Ser. E Tech. Sci.*, *51*(3), 308–322.

Zhang, S. R., X. Y. Huang, Y. Z. Su, and S. M. Radicella (1993), A physical model for one-dimension and time-dependent ionosphere. Part I: Description of the model, *Ann. Geofis.*, *36*, 105–110.

H. Le, L. Liu, B. Ning, W. Wan, and X. Yue, Beijing National Observatory of Space Environment, Institute of Geology and Geophysics, Chinese Academy of Sciences, No. 19 Beitucheng Xilu Chaoyang District, Beijing 100029, China. (lehj@mail.iggcas.ac.cn; liul@mail.iggcas.ac.cn; nbq@mail.iggcas.ac.cn; wanw@mail.iggcas.ac.cn; yuexinan@mail.iggcas.ac.cn)